Inorganic Chemistry

Article

pubs.acs.org/IC

# Roles of Acetone and Diacetone Alcohol in Coordination and Dissociation Reactions of Uranyl Complexes

Daniel Rios,[†,‡] George Schoendorff,[§,∥] Michael J. Van Stipdonk,[⊥] Mark S. Gordon,[§] Theresa L. Windus,*[,§] John K. Gibson,*[,†] and Wibe A. de Jong*[,#]

[†]Chemical Sciences Division, The Glenn T. Seaborg Center, Lawrence Berkeley National Laboratory, Berkeley, California 94720, United States

[§]Department of Chemistry, Iowa State University and Ames Laboratory, Ames, Iowa, 50011, United States

[⊥]Department of Chemistry, Lawrence University, Appleton, Wisconsin, 54911, United States

[#]EMSL, Pacific Northwest National Laboratory, P.O. Box 999, Richland, Washington 99352, United States

Supporting Information

**ABSTRACT:** Combined collision-induced dissociation mass spectrometry experiments with DFT and MP2 calculations were employed to elucidate the molecular structures and energetics of dissociation reactions of uranyl species containing acetone and diacetone alcohol ligands. It is shown that solutions containing diacetone alcohol ligands can produce species with more than five oxygen atoms available for coordination. Calculations confirm that complexes with up to four diacetone alcohol ligands can be energetically stable but that the effective number of atoms coordinating with uranium in the equatorial plane does not exceed five. Water elimination reactions of diacetone alcohol ligands are shown to have two coordination-dependent reaction channels, through formation of mesityl oxide ligands or formation of alkoxide and protonated mesityl oxide species. The present results provide an explanation for the implausible observation of "$[UO_2(ACO)_{6,7,8}]^{2+}$" in and observed water-elimination reactions from purportedly uranyl–acetone complexes (Rios, D.; Rutkowski, P. X.; Van Stipdonk, M. J.; Gibson, J. K. *Inorg. Chem.* **2011**, *50*, 4781).

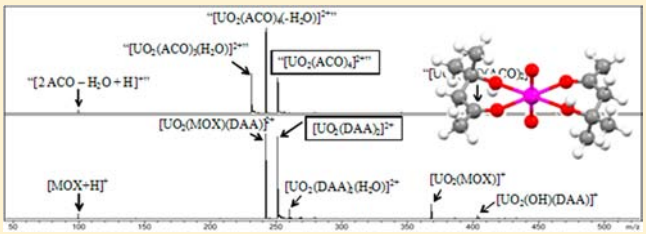


## INTRODUCTION

Understanding the coordination and reduction–oxidation chemistry of actinides is crucial for development and management of nuclear fuel cycles as well as nuclear waste storage sites. The coordination chemistry of the uranyl ion ($UO_2^{2+}$) has been studied extensively, both experimentally and with computer simulations. It is generally accepted that the coordination number (CN) for $UO_2^{2+}$ in the equatorial plane is five. A few exceptions are the strongly binding carbonate, nitrate, and acetate ions that form complexes in the solid phase and solution where six oxygen atoms coordinate with uranium in the equatorial plane.[1] Infrared multiphoton dissociation (IRMPD) experiments combined with density functional theory (DFT) calculations on tris-nitrate complexes of $UO_2^{2+}$ were able to show that six-coordinate anion species can also be produced in the gas phase.[2] In contrast, recent IRMPD experiments and DFT calculations on tris-carboxylate complexes of $UO_2^{2+}$ with acetate and benzoate showed that two of the acetate and benzoate ligands bound in a bidentate fashion, while the third acetate and benzoate were monodentate.[3] These results are more in line with the apparent preferred pentacoordination of the uranyl ion.

Hexa-, hepta-, or octacoordination in the equatorial plane of $UO_2^{2+}$ is not known, or expected, for monodentate neutral ligands such as acetone. Recent mass spectrometry experiments by some of us were performed with the successful primary goal of producing the first gas-phase dipositive plutonyl complexes.[4] In that work, ESI of uranyl acetone solutions produced species with $m/z$ ratios of 309, 338, and 367 for which there was no apparent explanation other than implausible "hypercoordinated" "$[UO_2(ACO)_{6,7,8}]^{2+}$" complexes.[4] Subsequent computational studies definitively showed that a first coordination shell (or inner sphere) with more than six acetones was energetically not feasible and that this explanation was incorrect.[5] Hydration experiments employing the same experimental conditions revealed that only inner-sphere coordination complexes are formed under these conditions,[6] ruling out the possibility that additional acetone molecules were forming a second solvation shell. The same mass spectrometry experiments revealed water-elimination processes, but as the dehydration of acetone is implausible the nature of the dehydration product was unknown.[4] Shvartsburg and Wilkes[7] demonstrated that CID of dipositive metal ion complexes comprising diacetone alcohol (DAA) ligands can induce aldol dehydration to produce mesityl oxide (MOX).

Electrospray ionization mass spectrometry experiments can identify species and reaction products by mass, but the exact

**Received:** July 20, 2012
**Published:** November 12, 2012





dx.doi.org/10.1021/ic3015964 | *Inorg. Chem.* 2012, 51, 12768–12775

molecular structure of the coordinating ligands is not necessarily resolved. This work describes an integrated experimental and computational effort to study the role of acetone and diacetone alcohol molecules in uranyl coordination and dissociation reactions. The work presented here, which was proposed in the previous experimental report,[4] provides a detailed picture of the composition and water-elimination reactions observed in the poorly understood "$[UO_2(ACO)_{6,7,8}]^{2+}$" species previously identified and disputes any speculation on the possibility of unusually high coordination numbers in gas-phase uranyl acetone coordination complexes.[4] None of the essential conclusions in ref 4 are affected by the new results.

## METHODOLOGIES

**Experimental Details.** The uranyl(VI) solutions for electrospray ionization (ESI) were prepared using a stock aqueous acidic solution of $^{238}U^{VI}O_2(ClO_4)_2$. The compositions of the ESI solutions were as follows: 180 $\mu$M $UO_2^{2+}$/0.1% $H_2O$/99.9% ACO (acetone); 180 $\mu$M $UO_2^{2+}$/0.1% $H_2O$/0.2% DAA (diacetone alcohol)/99.7% $d^6$ACO (perdeuterated acetone); and 180 $\mu$M $UO_2^{2+}$/0.1% $H_2O$/0.2% $d^{12}$DAA (perdeuterated DAA)/99.7% ACO. All handling of the uranium solutions (>99% $^{238}U$) was performed in a radiological laboratory. ESI and ion−molecule reactions were studied using an Agilent 6340 Quadrupole Ion Trap Mass Spectrometer (QIT/MS) with the ion source located inside of a radiological containment glovebox, as described in detail elsewhere.[4,8] The sequential multistage mass spectrometry ($MS^n$) collision-induced dissociation (CID) capabilities of the QIT/MS allow for isolation of ions with a particular mass-to-charge ratio, $m/z$, followed by resonant variable-energy excitation, which results in multiple energetic collisions of the selected ion with the He bath gas and ultimately in ion decomposition/fragmentation by one or more pathways. CID fragmentation products are determined by mass-selective ion ejection from the trap into an electron multiplier detector. The effective ion temperature in the trap prior to CID is estimated as ~300 K.[9]

In high-resolution mode the QIT/MS has a detection range of 50−2200 $m/z$ and a resolution of ~0.25 $m/z$ (full width half-maximum). Mass spectra were acquired in the positive-ion accumulation and detection mode using the following typical ESI, desolvation, ion transport/focusing, and ion trapping parameters: nebulizer gas pressure, 12 psi; capillary voltage and current, −4500 V, 1.221 nA; end plate voltage offset and current, −500 V, 22.5 nA; dry gas flow rate, 5 L/min; dry gas temperature, 100 °C; capillary exit, 75 V; skimmer, 29.2 V; octopole 1 and 2 DC, 11.46 and 7.40 V; octopole RF amplitude, 50.0 Vpp; lens 1 and 2, −2.3 and −77.5 V; trap drive, 49.9. The parameters were somewhat different for selected spectra, where the conditions were optimized to enhance a particular low-intensity species. Solutions were injected into the electrospray capillary via a syringe pump at a rate of 60 $\mu$L min$^{-1}$. Nitrogen gas for nebulization and drying in the ion transfer capillary was supplied by the boil-off from a liquid nitrogen dewar. CID experiments were performed using the He buffer gas. The ion tickling voltages ranged between 0.35 and 0.50 V, applied for 40 ms; the CID voltage was selected to provide a suitable depletion of the precursor and adequate abundances of the CID products. Pressures in the trap were ~$10^{-4}$ Torr helium buffer gas and ~$10^{-6}$ Torr background water.[6] For preparation of $[UO_2(ACO)_4]^{2+}$ from $[UO_2(ACO)_3(H_2O)]^{2+}$, the ACO reagent was introduced from a liquid reservoir into the same gas inlet through which the He buffer gas was injected into the ion trap; the ACO pressure was controlled by a variable leak valve.

All organic reagents were commercial products with a purity of 99.9%, except for 99% DAA alcohol. The isotopic purity of the $d^6$ACO was reported as 99.97 atom % D and that of the $d^{12}$DAA was 98 atom % D. The ACO introduced into the ion trap as a gas was subjected to freeze−vacuum−thaw cycles of the ACO source liquid prior to use to eliminate volatile impurities.

As DAA is indistinguishable from $(ACO)_2$ by mass spectrometry, a key aspect of the experiments was to ensure the identity of the ligands using deuterated $d^6$ACO and $d^{12}$DAA. The isolated $[UO_2(DAA)(d^6ACO)_2]^{2+}$, $[UO_2(DAA)_2(d^6ACO)]^{2+}$, $[UO_2(DAA)_2(d^6ACO)_2]^{2+}$, $[UO_2(DAA)_2]^{2+}$, and $[UO_2(DAA)_3]^{2+}$ complex ions were prepared from the DAA/$d^6$ACO solution. The $[UO_2(d^{11}DAA)(ACO)_3]^{2+}$ complex ion was prepared from the $d^{12}$DAA/ACO solution; solution and/or gas-phase exchange of the alcohol D atom in $d^{12}$DAA accounts for complete conversion to $d^{11}$DAA. The $[UO_2(ACO)_4]^{2+}$ complex ion was prepared using the pure ACO solution as follows: the isolated $[UO_2(ACO)_3(H_2O)]^{2+}$ complex ion was exposed to ~$10^{-6}$ Torr ACO gas in the ion trap for 500 ms such that the $H_2O$ ligand was replaced by the stronger base ACO; the $[UO_2(ACO)_4]^{2+}$ product was then isolated and subjected to CID.

**Computational Details.** All electronic structure calculations were performed using the NWChem computational chemistry software.[10] For uranium the small core Stuttgart effective core potential and associated basis set was used,[11−13] while the remaining elements (O, C, and H) were described with the DFT-optimized valence triple-$\zeta$ plus polarization (TZVP) basis set.[14] Throughout the calculations spherical basis functions were used.

All structures and frequencies were obtained using the local density approximation (LDA).[15,16] While there are many different conformers of the ligands, only the lowest energy structures are used in this study. All binding and reaction energies reported at the MP2 level of theory were obtained using these LDA-optimized structures. In the MP2 calculations, the 1s core orbitals for O and C were frozen. All energies include the zero-point energy correction obtained from the LDA frequency calculations. Additional energetics obtained with the B3LYP[17,18] and SSB-D[19] functionals are included in the Supporting Information. The trends in binding energies for both B3LYP and SSB-D functionals are the same as MP2. B3LYP tends to underbind the ligands, especially for species with larger numbers of ligands, whereas the SSB-D energies seem to provide binding energies that are in good agreement with those obtained with MP2.

## RESULTS AND DISCUSSION

**Revealing the Compositions of "Uranyl Acetone" Complexes by CID.** Gas-phase uranyl complexes comprised of precisely known normal or deuterium-labeled ACO and/or DAA ligands were prepared by ESI and subjected to CID. The results were compared with those previously obtained from ESI of uranyl in "pure acetone".[4] Comparison of the CID results with those for ESI complexes from nominally high-purity ACO provides an assessment of the role of DAA in complex formation and fragmentation. Throughout the discussion of the experimental results, species in quotation marks refer to those prepared by ESI from "pure acetone", with indeterminate compositions; species identified without quotation marks were prepared as described in the Experimental Details and have the indicated ligand compositions.

In evaluating the CID results, aldol dehydration and dissociation of DAA are considered as possible processes. DAA dehydration to MOX is given by eq 1a and dissociation to two ACO by eq 1b, where deuterium labeling is employed to track the alcohol H atom in $d^{11}$DAA and $d^{10}$MOX is the product in eq 1a

$$CD_3C(O)CD_2C(OH)(CD_3)_2 \rightarrow CD_3C(O)CD{=}C(CD_3)_2 + HDO \quad (1a)$$

$$CD_3C(O)CD_2C(OH)(CD_3)_2 \rightarrow CD_3C(O)CD_2H + CD_3C(O)CD_3 \quad (1b)$$

In CID of coordination complexes such as $[UO_2(ACO)_n]^{2+}$, the predominant process is typically ligand elimination, loss of


dx.doi.org/10.1021/ic3015964 | Inorg. Chem. 2012, 51, 12768−12775

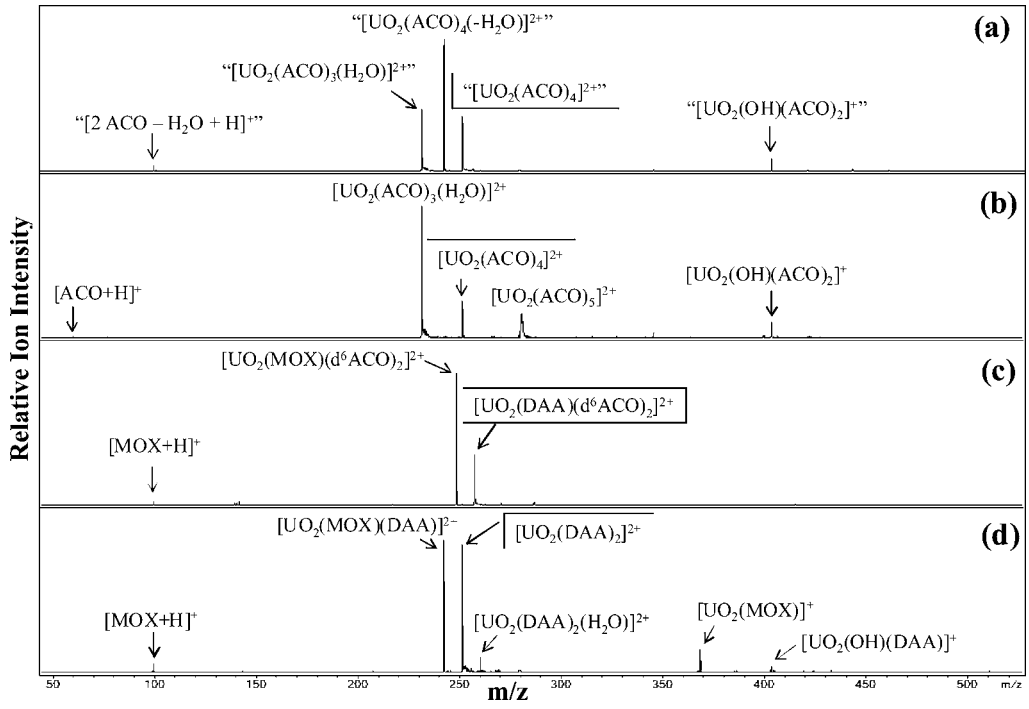


**Figure 1.** CID product spectra for precursor ions (identified in boxes) with an equatorial coordination number of 4. (a) Species with $m/z$ = 251, which corresponds to "$[UO_2(ACO)_4]^{2+}$", produced from nominally "pure acetone"; all species are in quotes as the ligand compositions were not known. (b–d) Species with the same atomic composition as a but with known ligand compositions; use of deuterated ACO in c enabled definitive ligand identification. $[UO_2(ACO)_5]^{2+}$ product peak in b results not from CID but rather from gas-phase addition of ACO, which was necessarily present in the ion trap to prepare the precursor ion. Species identified as $[UO_2(ACO)_4(-H_2O)]^{2+}$ in a is revealed to be $[UO_2(MOX)(ACO)_2]^{2+}$ from these results.

an ACO ligand in this case. If the $[UO_2(ACO)_{n-1}]^{2+}$ product is sufficiently undercoordinated, addition of background water in the gas phase can occur to produce $[UO_2(ACO)_{n-1}(H_2O)]^{2+}$. The results in Figure 1 show ligand elimination and hydration as the dominant processes for elementary uranyl ACO coordination complexes. Other processes reveal the presence of other types of ligands and more complex fragmentation processes.

In Figure 1 are shown spectra for uranyl complexes in which the presumed coordination number is four: "$[UO_2(ACO)_4]^{2+}$" prepared by ESI from "pure acetone", $[UO_2(ACO)_4]^{2+}$, $[UO_2(DAA)(d^6ACO)_2]^{2+}$, and $[UO_2(DAA)_2]$, where the last three of these were prepared as described in the Experimental Details section. Comparison of the CID spectrum of "$[UO_2(ACO)_4]^{2+}$" (Figure 1a) with that of $[UO_2(ACO)_4]^{2+}$ (Figure 1b) clearly reveals that identification of the former as a uranyl acetone complex is inaccurate. In particular, $[UO_2(ACO)_4]^{2+}$ exhibits almost exclusively ACO ligand loss, with rapid addition of background water to undercoordinated $[UO_2(ACO)_3]^{2+}$ to produce $[UO_2(ACO)_3(H_2O)]^{2+}$ according to eq 2a′; no $H_2O$ elimination appears for this species, the absence of which confirms that this is the true $[UO_2(ACO)_4]^{2+}$ complex. It should be remarked that the small peak assigned as $[UO_2(ACO)_5]^{2+}$ results from ACO addition, not CID. As gaseous ACO was present in the trap for this experiment to prepare pure $[UO_2(ACO)_4]^{2+}$, the precursor ion was presumably regenerated according to eq 2b, with the result that the apparent CID yields in Figure 1b underrepresented the contribution from ACO elimination.

$$[UO_2(ACO)_4]^{2+} \rightarrow [UO_2(ACO)_3]^{2+} + ACO \quad (2a)$$

$$[UO_2(ACO)_3]^{2+} + H_2O \rightarrow [UO_2(ACO)_3(H_2O)]^{2+} \quad (2a')$$

$$[UO_2(ACO)_3]^{2+} + ACO \rightarrow [UO_2(ACO)_4]^{2+} \quad (2b)$$

CID of $[UO_2(DAA)(d^6ACO)_2]^{2+}$ (Figure 1c) resulted almost exclusively in dehydration to produce $[UO_2(MOX)(ACO)_2]^{2+}$ according to eq 3.

$$[UO_2(DAA)(d^6ACO)_2]^{2+} \rightarrow [UO_2(MOX)(d^6ACO)_2]^{2+} + H_2O \quad (3)$$

It is evident that $[UO_2(DAA)(ACO)_2]^{2+}$ would account for the appearance of the $[UO_2(ACO)_4(-H_2O)]^{2+}$ product, i.e., $[UO_2(MOX)(ACO)_2]^{2+}$, from "$[UO_2(ACO)_4]^{2+}$". The CID spectrum for $[UO_2(DAA)_2]^{2+}$ (Figure 1d) indicates that the predominant process is dehydration as given by eq 4.

$$[UO_2(DAA)_2]^{2+} \rightarrow [UO_2(MOX)(DAA)]^{2+} + H_2O \quad (4)$$

The CID spectrum of $[UO_2(DAA)_2]^{2+}$ also includes smaller but distinct peaks corresponding to $[UO_2(DAA)_2(H_2O)]^{2+}$ and $[UO_2(MOX)]^{+}$, which do not appear in the "$[UO_2(ACO)_4]^{2+}$" CID mass spectrum. We thus conclude that "$[UO_2(ACO)_4]^{2+}$" produced by ESI from "pure acetone" is primarily comprised of $[UO_2(ACO)_4]^{2+}$ and $[UO_2(DAA)(ACO)_2]^{2+}$.

The source of DAA ligands in complexes prepared from purportedly pure ACO is uncertain. Although the coupling of two ACO ligands in gas-phase uranyl complexes could lead to formation of DAA ligands, a more plausible source is DAA as a known inherent impurity in acetone.[20,21] The concentration of DAA should be enhanced with addition of acidic aqueous uranyl ion to acetone.[22] The yields of DAA complexes from ESI


dx.doi.org/10.1021/ic3015964 | Inorg. Chem. 2012, 51, 12768–12775

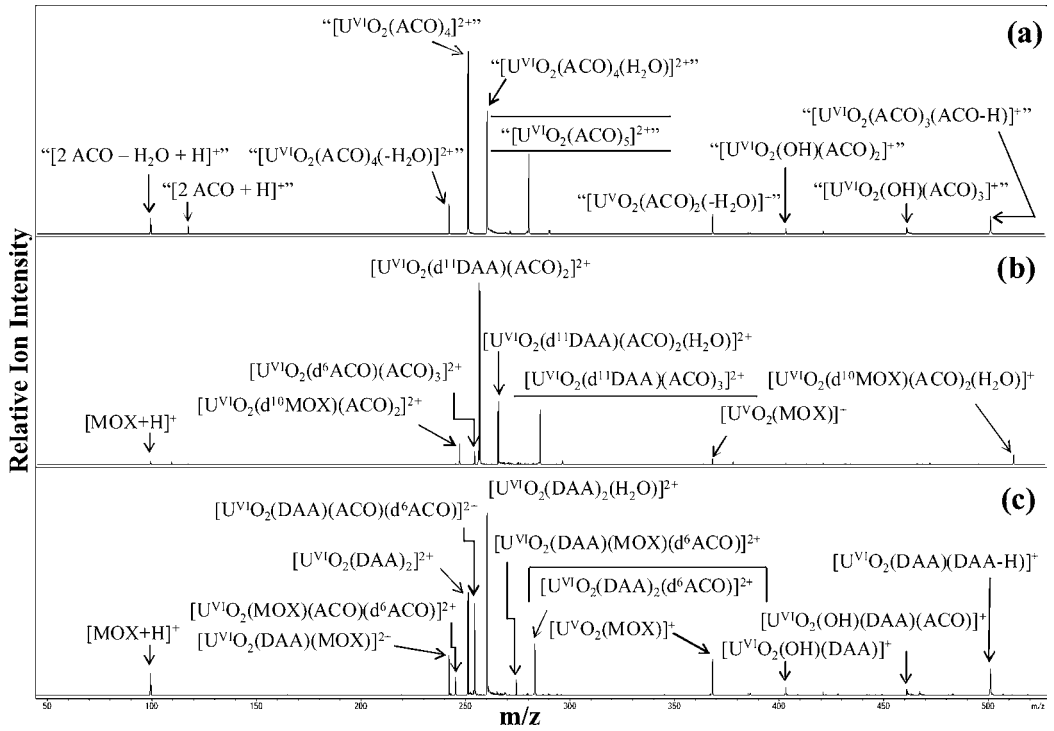


**Figure 2.** CID product spectra for precursor ions (identified in boxes) with an equatorial coordination number of 5. (a) Species with $m/z$ = 280, which corresponds to "$[UO_2(ACO)_5]^{2+}$", produced from nominally "pure acetone". (b and c) Species with the same atomic composition as a but with known ligand compositions; use of deuterated DAA in b and deuterated ACO in c enabled definitive ligand identification.

of acetone solutions to which 0.2% DAA or $d^{12}$DAA had been added suggest that a concentration of ∼0.1% DAA in acetone would be adequate to account for the observed ESI yield of $[UO_2(DAA)(ACO)_2]^{2+}$ as well as the other DAA complexes discussed below. The appearance of DAA in ESI complexes at such low solution concentrations is attributed to the high basicity of DAA and its ability to exhibit bidentate coordination.

The presence of DAA in "$[UO_2(ACO)_5]^{2+}$" produced by ESI from "pure acetone" is consistent with the CID results shown in Figure 2. In contrast to $[UO_2(ACO)_4]^{2+}$, there is no convenient route to produce pure gas-phase $[UO_2(ACO)_5]^{2+}$, which may not be stable in the ion trap under the experimental conditions; accordingly, only the two DAA-substituted complexes with atomic compositions corresponding to "$[UO_2(ACO)_5]^{2+}$" were studied. The dominant CID pathways for $[UO_2(d^{11}DAA)(ACO)_3]^{2+}$ (Figure 2b) are given by eqs 5a–5c, where eq 5a′ is hydration of the ligand-loss product in eq 5a; minor channels resulted in monopositive MOX products identified in Figure 2b.

$$[UO_2(d^{11}DAA)(ACO)_3]^{2+} \rightarrow [UO_2(d^{11}DAA)(ACO)_2]^{2+} + ACO \quad (5a)$$

$$[UO_2(d^{11}DAA)(ACO)_2]^{2+} + H_2O \rightarrow [UO_2(d^{11}DAA)(ACO)_2(H_2O)]^{2} \quad (5a')$$

$$[UO_2(d^{11}DAA)(ACO)_3]^{2+} \rightarrow [UO_2(d^{6}ACO)(ACO)_3]^{2+} + d^5ACO \quad (5b)$$

$$[UO_2(d^{11}DAA)(ACO)_3]^{2+} \rightarrow [UO_2(d^{10}MOX)(ACO)_2]^{2+} + ACO + HDO \quad (5c)$$

The appearance of exclusively $d^{10}$MOX with elimination of HDO (eq 5c) is consistent with the presumed composition of $d^{11}$DAA as $CD_3(O)CD_2C(OH)(CD_3)_2$ (eq 1a). The exclusive appearance of $[UO_2(d^6ACO)(ACO)_3]^{2+}$ with $d^5$ACO elimination (eq 5b) indicates a particular coordination to the uranium metal center during DAA dissociation (eq 1b). Some CID pathways seen for $[UO_2(DAA)_2(d^6ACO)]^{2+}$ in Figure 2c are given by eqs 6a–6d, where eq 6a′ is hydration of the ligand-loss product from eq 6a.

$$[UO_2(DAA)_2(d^6ACO)]^{2+} \rightarrow [UO_2(DAA)_2]^{2+} + d^6ACO \quad (6a)$$

$$[UO_2(DAA)_2]^{2+} + H_2O \rightarrow [UO_2(DAA)_2(H_2O)]^{2+} \quad (6a')$$

$$[UO_2(DAA)_2(d^6ACO)]^{2+} \rightarrow [UO_2(DAA)(ACO)(d^6ACO)]^{2+} + ACO \quad (6b)$$

$$[UO_2(DAA)_2(d^6ACO)]^{2+} \rightarrow [UO_2(DAA)(MOX)]^{2+} + d^6ACO + H_2O \quad (6c)$$

$$[UO_2(DAA)_2(d^6ACO)]^{2+} \rightarrow [UO_2(DAA)(MOX)(d^6ACO)]^{2+} + H_2O \quad (6d)$$

$$[UO_2(DAA)_2(d^6ACO)]^{2+} + H_2O \rightarrow [UO_2(DAA)(DAA-H)]^{+} + d^6ACO + [H_3O]^{+} \quad (6e)$$

The postulated $[H_3O]^+$ product ion in eq 6e would not be detected due to the low mass cutoff of the mass spectrometer. The $[UO_2(MOX)(ACO)_2]^{2+}$ product in Figure 2a corresponds to $[UO_2(d^{10}MOX)(ACO)_2]^{2+}$ in Figure 2b and $[UO_2(DAA)$-


dx.doi.org/10.1021/ic3015964 | Inorg. Chem. 2012, 51, 12768–12775

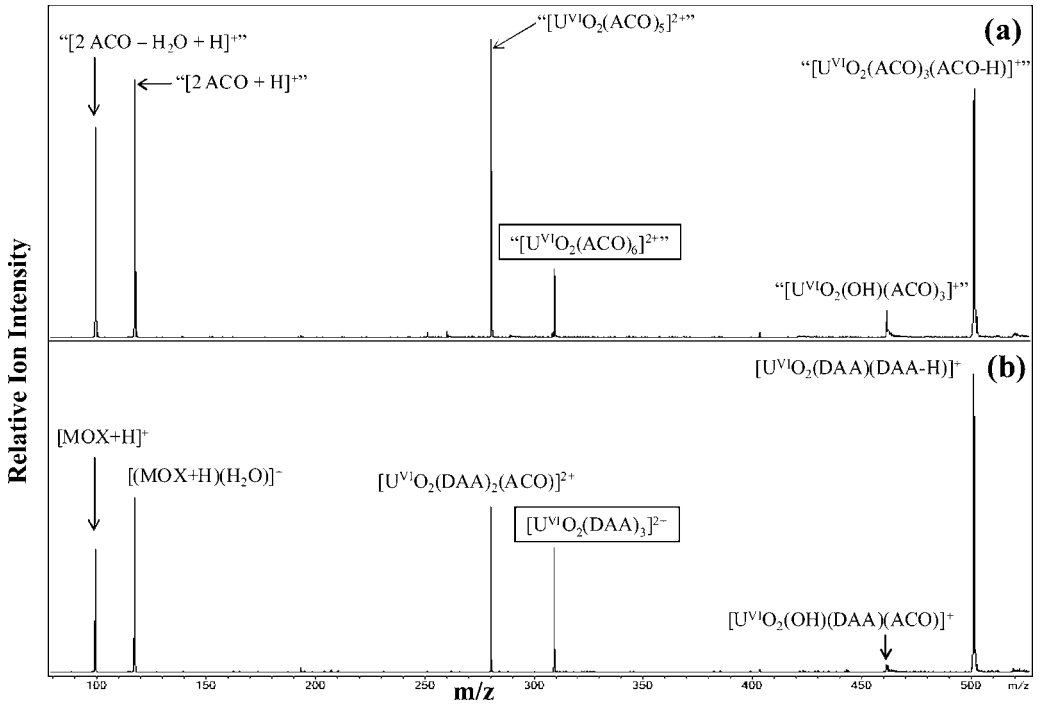


**Figure 3.** CID product spectra for precursor ions (identified in boxes) with a nominal equatorial coordination number of 6. (a) Species with $m/z$ = 309, which corresponds to "$[UO_2(ACO)_6]^{2+}$", produced from nominally "pure acetone". (b) Species with the same atomic composition as a but with known ligand composition $[UO_2(DAA)_3]^{2+}$.

$(MOX)]^{2+}$ in Figure 2c, indicating that "$[UO_2(ACO)_5]^{2+}$" prepared from "pure acetone" comprises $[UO_2(DAA)(ACO)_3]^{2+}$ and/or $[UO_2(DAA)_2(ACO)]^{2+}$. The comparable yields in Figure 2a and 2c of $[MOX + H]^+$ and $[UO_2(MOX)]^+$, which result from CID processes which are less obvious than those presented in eqs 6a–6d, suggest a significant amount of $[UO_2(DAA)_2(ACO)]^{2+}$ in "$[UO_2(ACO)_5]^{2+}$". As all of the peaks in the "$[UO_2(ACO)_5]^{2+}$" CID spectrum can be attributed to the DAA-containing complexes, it is feasible that little, if any, of the true penta-acetone complex, $[UO_2(ACO)_5]^{2+}$, is present in "$[UO_2(ACO)_5]^{2+}$". Both direct ligand loss (eqs 5a and 6a) and retro-aldol DAA dissociation followed by ligand loss (eqs 5b and 6b) could account for the observed elimination of ACO from "$[UO_2(ACO)_5]^{2+}$".

The appearance of "$[UO_2(ACO)_6]^{2+}$" from "pure acetone" suggested an untenable coordination number of six; the appearance of "$[UO_2(ACO)_7]^{2+}$" and "$[UO_2(ACO)_8]^{2+}$" were even more problematic.[4] With the knowledge that DAA was present in other complexes, we speculated that DAA ligands also accounted for these complexes. In Figure 3 are shown the CID spectra for "$[UO_2(ACO)_6]^{2+}$" and $[UO_2(DAA)_3]^{2+}$. The CID processes in Figure 3b are given by eqs 7a and 7b; hydration of $[MOX + H]^+$ from eq 7b results in $[(MOX + H)(H_2O)]^+$. A very small peak corresponding to $[UO_2(OH)(DAA)(ACO)]^+$ also appeared (Figure 3b), but the process leading to this minor product is speculative.

$$[UO_2(DAA)_3]^{2+} \rightarrow [UO_2(DAA)_2(ACO)]^{2+} + ACO \quad (7a)$$

$$[UO_2(DAA)_3]^{2+} \rightarrow [UO_2(DAA)(DAA - H)]^+ + [MOX + H]^+ + H_2O \quad (7b)$$

It was possible to prepare only a small amount of $[UO_2(DAA)_2(d^6ACO)_2]^{2+}$ to isolate for CID. The resulting CID spectrum was poor quality, but the processes in eqs 8a and 8b were identified.

$$[UO_2(DAA)_2(d^6ACO)_2] \rightarrow [UO_2(DAA)(ACO)(d^6ACO)_2]^{2+} + ACO \quad (8a)$$

$$[UO_2(DAA)_2(d^6ACO)_2] \rightarrow [UO_2(DAA)_2(d^6ACO)]^{2+} + d^6ACO \quad (8b)$$

The appearance of monopositive MOX products from "$[UO_2(ACO)_6]$" indicated the presence of a DAA ligand in some complexes. Substantial retro-aldol dissociation of DAA to two ACO ligands, concomitant with ACO ligand loss, appeared in CID of both $[UO_2(DAA)_3]^{2+}$ (eq 7a) and $[UO_2(DAA)_2(d^6ACO)_2]$ (eq 8a). The abundance of the ACO-loss product from $[UO_2(DAA)_3]^{2+}$ was less than that from "$[UO_2(ACO)_6]^{2+}$", indicating the presence in the latter of $[UO_2(DAA)_2(ACO)_2]^{2+}$ and/or $[UO_2(DAA)(ACO)_4]^{2+}$. No dipositive uranyl MOX complexes appeared for "$[UO_2(ACO)_6]^{2+}$", $[UO_2(DAA)_3]^{2+}$, or $[UO_2(DAA)_2(d^6ACO)_2]^{2+}$ rather only monopositive MOX products such those seen in Figure 3. Aldol dehydration of DAA to MOX in high-coordination complexes evidently results in charge separation with elimination of protonated MOX; deprotonation of DAA results in an alkoxide ligand such that the U(VI) oxidation state is retained. The key conclusion is that "$[UO_2(ACO)_6]$" is a complex which comprises one or more DAA ligands and does not comprise weakly bound outer-sphere ACO molecules. We further infer that the previously identified "$[UO_2(ACO)_7]$" and "$[UO_2(ACO)_8]$" complexes prepared from ESI of "pure acetone"[4] are formed from DAA ligands.

**Calculations of Uranyl DAA Complexes: Comparing Experiment and Theory.** DFT and MP2 calculations were


dx.doi.org/10.1021/ic3015964 | Inorg. Chem. 2012, 51, 12768–12775

performed to validate the experimental observations and gain insight into the coordination structure and binding energies of these $UO_2^{2+}$ species. All calculated geometries and raw energetic information are available in the Supporting Information.

**ACO/DAA Species.** Both the ACO and the DAA ligands form bonds with uranium in the equatorial plane through their oxygen atoms. The DAA ligand can form up to two bonds, either coordinating in a monodentate or bidentate fashion. Figure 4 shows the LDA-optimized structures for four different

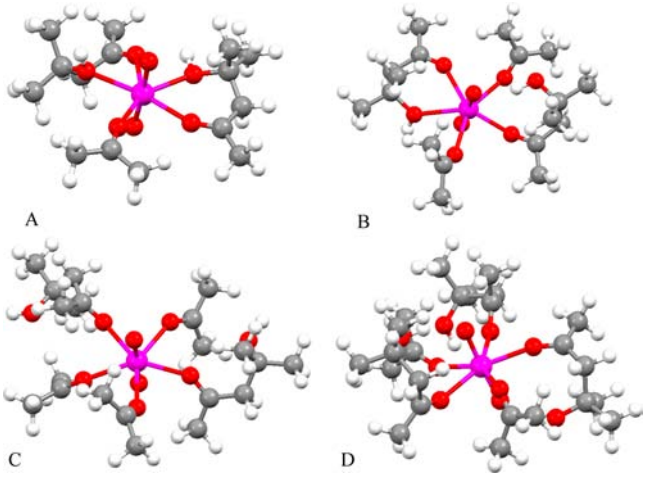


**Figure 4.** Subset of optimized structures of $UO_2^{2+}$ species with five or more DAA and/or ACO ligand oxygens. Uranium is shown in magenta, oxygen is red, carbon is gray, and hydrogen is white. $[UO_2(ACO)_1(DAA)_2]^{2+}$ (A); $[UO_2(ACO)_2(DAA)_2]^{2+}$ (B); $[UO_2(ACO)_3(DAA)_2]^{2+}$ (C); $[UO_2(ACO)_2(DAA)_3]^{2+}$ (D).

$UO_2^{2+}$ species with 5, 6, 7, and 8 ligand-based oxygen atoms. Generally, the ACO and DAA ligands prefer to lie in the equatorial plane around the uranium with the uranyl being close to linear. Due to its asymmetric structure, the DAA ligands are slightly bent out of plane (U−O−C angle 4−5° out of plane).

Table 1 summarizes the coordination numbers of the equatorial oxygen atoms in the mixed $[UO_2(ACO)_x(DAA)_y]^{2+}$

**Table 1. Coordination of Ligand Oxygens with Uranium in the Equatorial Plane**[a]

| species | $CN_{U-O}(DAA)$ | $CN_{U-O}(eq)$ |
|---|---|---|
| $[UO_2(DAA)_1]^{2+}$ | 2 | 2 |
| $[UO_2(ACO)_1(DAA)_1]^{2+}$ | 2 | 3 |
| $[UO_2(ACO)_2(DAA)_1]^{2+}$ | 2 | 4 |
| $[UO_2(ACO)_3(DAA)_1]^{2+}$ | 2 | 5 |
| $[UO_2(ACO)_4(DAA)_1]^{2+}$ | 1 | 5 |
| $[UO_2(DAA)_2]^{2+}$ | 4 | 4 |
| $[UO_2(ACO)_1(DAA)_2]^{2+}$ | 4 | 5 |
| $[UO_2(ACO)_2(DAA)_2]^{2+}$ | 3 | 5 |
| $[UO_2(ACO)_3(DAA)_2]^{2+}$ | 2 | 5 |
| $[UO_2(DAA)_3]^{2+}$ | 5 | 5 |
| $[UO_2(ACO)_1(DAA)_3]^{2+}$ | 4 | 5 |
| $[UO_2(ACO)_2(DAA)_3]^{2+}$ | 3 | 5 |
| $[UO_2(DAA)_4]^{2+}$ | 5 | 5 |

[a] $CN_{U-O}(DAA)$ is the number of DAA-oxygen atoms coordinating with uranium; $CN_{U-O}(eq)$ is the total number of coordinating oxygen atoms in the equatorial plane.

species. Overall, the highest U−O coordination in the equatorial plane for all of the calculated DAA/ACO species was found to be 5, in accord with the general consensus on the coordination of ligands with $UO_2^{2+}$. The DAA ligands form bidentate bonds to maximize the equatorial coordination with the uranium up to five bonds where possible (see Table 1). For species with 1−5 oxygen atoms coordinating with uranium in the equatorial plane this is definitely the case. When six or more ligand oxygen atoms can coordinate, DAA ligands resort to binding in a monodentate manner with the weaker bonding alcohol group not coordinating with the uranium. A structure with all three ligands binding in a bidentate fashion was found for the $[UO_2(DAA)_3]^{2+}$ species, about 2.5 kcal/mol higher in energy at the MP2 level of theory, suggesting this coordination might be observed in experiment.

Figure 5 shows the relative MP2 binding energies for successive addition of ACO or DAA using the lowest energy structure found for any given complex. The calculated binding energies show that stable species with the equivalent of up to eight ACO molecules can be formed from a combination of DAA and ACO ligands. Addition of either ACO or DAA is an exoergic process. The data in Figure 5 shows that the presence of small amounts of DAA in the experiments will lead to formation of DAA-containing complexes as deduced from the experiments described above. On the basis of the calculated relative binding energies, we postulate that the observed "$[UO_2(ACO)_8]^{2+}$" species can only be formed as $[UO_2(DAA)_4]^{2+}$ with one DAA ligand binding in a bidentate manner and three DAA ligands binding in a monodentate fashion.

Also shown in Figure 5 is the addition and dimerization of ACO resulting in formation of a DAA ligand. This process is generally less favorable than addition of either the DAA or the ACO ligand. However, the dimerization process does become competitive, and in some cases favorable, with simple ACO addition for species with five or more oxygen atoms available for bonding in the equatorial plane. Together with the observation that DAA ligands are present in the gas-phase experiments, this provides strong evidence that the previously observed "$[UO_2(ACO)_6]^{2+}$", "$[UO_2(ACO)_7]^{2+}$", and "$[UO_2(ACO)_8]^{2+}$" species[4] were actually complexes which comprised one or more DAA ligands and exhibited coordination numbers that did not exceed five.

**CID Species.** A summary of the calculated reaction energies for the four main CID channels of the precursor species studied computationally is shown in Table 2. These are detachment of DAA, loss of ACO through detachment of ACO or decomposition of a DAA ligand, formation of mesityl oxide (MOX) and associated loss of $H_2O$, and formation of an alkoxide $(DAA - H)^+$ combined with $(MOX + H)^+$ formation and water loss. Overall, the reaction energetics calculated for these CID channels align well with the experimental observations. The only exceptions are the MOX formation for $[UO_2(DAA)_3]^{2+}$ and alkoxide formation process for $[UO_2(DAA)_2]^{2+}$, which will be discussed later.

Loss of a DAA ligand during the CID process is found to be a high-energy process relative to other product channels, clearly explaining why this process is not observed in the experiments. To detach the DAA molecule enough energy needs to be injected into the molecule for two uranium−ligand bonds to be broken. As discussed before, $[UO_2(DAA)_3]^{2+}$ might have two bidentate- and one monodentate-bonded DAA ligand. However, over 58 kcal/mol of energy is required to detach the DAA


dx.doi.org/10.1021/ic3015964 | Inorg. Chem. 2012, 51, 12768−12775

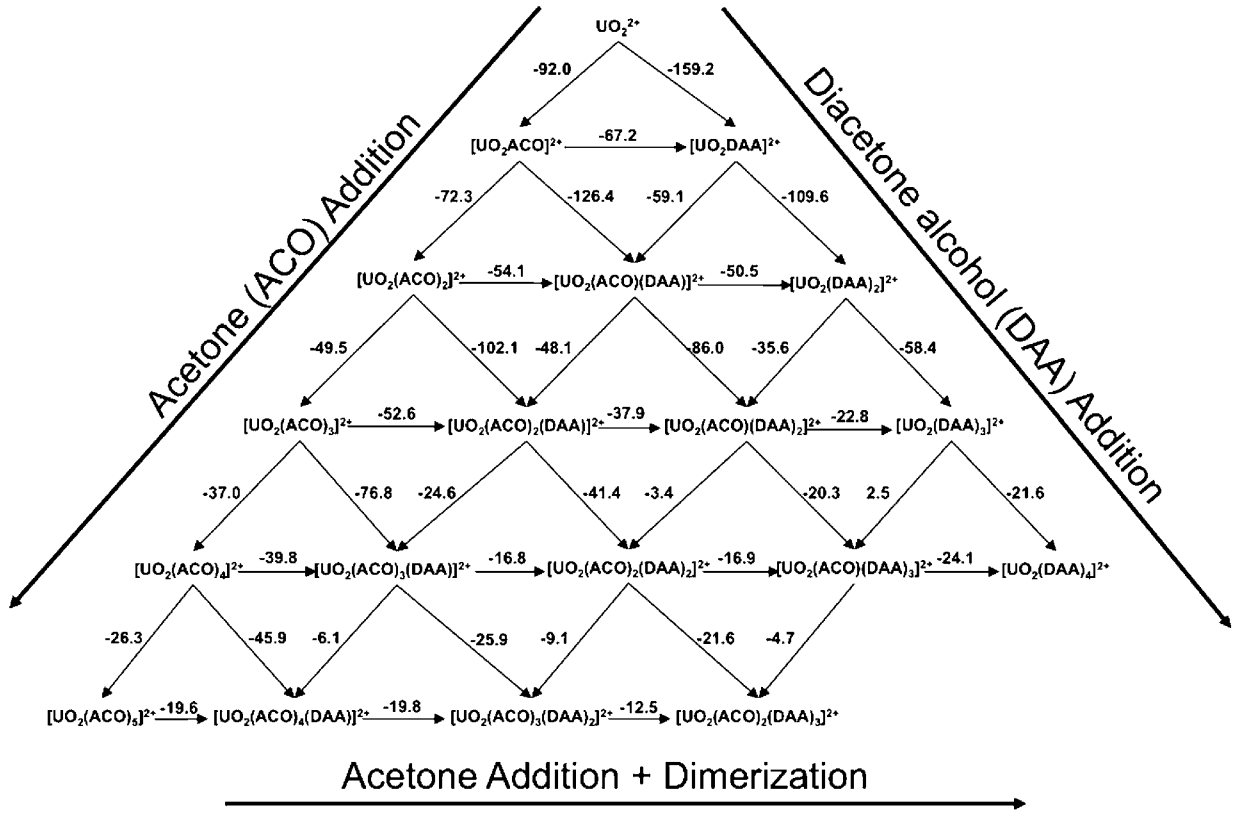


**Figure 5.** Relative binding energies at the MP2 level of theory (units are kcal/mol, geometries were obtained using LDA) for addition of acetone ($[UO_2(ACO)_x(DAA)_y]^{2+}$ + ACO → $[UO_2(ACO)_{x+1}(DAA)_y]^{2+}$), diacetone alcohol ($[UO_2(ACO)_x(DAA)_y]^{2+}$ + DAA → $[UO_2(ACO)_x(DAA)_{y+1}]^{2+}$), and acetone with dimerization ($[UO_2(ACO)_x(DAA)_y]^{2+}$ + ACO → $[UO_2(ACO)_{x-1}(DAA)_{y+1}]^{2+}$). Energies for acetone addition with dimerization include the energy for formation of DAA from two ACO ligands (approximately −10.8 kcal/mol).

**Table 2. Calculated Dissociation Energies at the MP2 Level of Theory (units are kcal/mol) and Experimental CID Channels Observed for Selected $UO_2^{2+}$ Species, Ordered by Their Coordination Number (CN) in the Equatorial Plane[a]**

| | | loss of ACO | | | | | | | | | |
|---|---|---|---|---|---|---|---|---|---|---|---|
| precursor species[b] | | DAA → $(ACO)_2$ | | ACO loss | | loss of DAA (DAA ligand loss) | | loss of $H_2O$ (DAA → MOX) | | alkoxide formation $(DAA-H)^+$ (MOX + $H)^+$ and $H_2O$ loss | |
| CN | | calcd | exp | calcd | exp | calcd | exp | calcd | exp | calcd | exp |
| 6 | $(DAA)_3$ | 12.0 | Y | | | 58.4 | N | 12.7 | N | 10.8 | Y |
| 5 | $(ACO)_1(DAA)_2$ | 27.1 | Y | 35.6 | Y | 86.0 | N | 26.6 | Y | 25.2 | Y |
| | $(ACO)_3(DAA)_1$ | 29.0 | Y | 24.6 | Y | 76.8 | N | 23.2 | Y | | |
| 4 | $(DAA)_2$ | 39.6 | N | | | 109.6 | N | 33.4 | Y | 20.9 | N |
| | $(ACO)_2(DAA)_1$ | 41.4 | N | 48.1 | N | 102.1 | N | 31.5 | Y | | |

[a]Y indicates that the CID channel was experimentally observed; N indicates that the channel was not observed. [b]Isotopic compositions of the species employed for the CID experiments are as indicated in Figures 1−3.

ligand. The data in Figure 5 predict that DAA loss would be observed for species with additional ACO or DAA ligands. Loss of an ACO ligand can occur through either detachment of an ACO ligand or decomposition of a DAA ligand. The latter process is the only process available for the $DAA_n$ species. In most of the mixed ACO/DAA species the DAA decomposition process is slightly favored over detachment of an ACO ligand. The energy required to lose an ACO decreases as the coordination number increases, which can be attributed to weakening of the primarily electrostatic bonding between the ligands and uranyl (see ref 23 for a more detailed discussion on the role of charge delocalization on the bonding of uranyl with ligands). No ACO loss processes were observed for $[UO_2(DAA)_2]^{2+}$ and $[UO_2(ACO)_2(DAA)_1]^{2+}$ with a coordination number of four. As can be seen in Table 2, either loss of $H_2O$ or alkoxide formation is a lower energy process for these species, whereas these processes are competitive with the ACO loss for species with coordination numbers of five and six. The calculated results in Table 2 also suggest that less than the necessary 40 kcal/mol of thermal energy needed to dissociate an ACO from $[UO_2(DAA)_2]^{2+}$ or $[UO_2(ACO)_2(DAA)_1]^{2+}$ was injected into the species under the experimental CID conditions in this work.

Alkoxide formation and loss of water through formation of a MOX ligand are found to be favorable for all species studied in this work. However, experimentally no MOX formation was observed for $[UO_2(DAA)_3]^{2+}$ and no alkoxide formation was observed for $[UO_2(DAA)_2]^{2+}$. Both reactions are not simple


dx.doi.org/10.1021/ic3015964 | Inorg. Chem. 2012, 51, 12768−12775

dissociation processes, and the complex mechanisms most likely involve multiple steps with transition states and associated barriers and dynamical processes driving reaction probabilities. For $[UO_2(DAA)_2]^{2+}$ the process might occur through dissociation of OH from DAA, with subsequent extraction of a hydrogen by the OH group from the same ligand. A similar mechanism can be postulated for the $[UO_2(ACO)_1(DAA)_2]^{2+}$ and $[UO_2(DAA)_3]^{2+}$ precursor species, where the hydrogen gets extracted (solely in the case of $[UO_2(DAA)_3]^{2+}$) from another DAA ligand, resulting in formation of alkoxide products. The shift from pure MOX to alkoxide with the increased coordination number suggests that the crowding of ligands affects the reaction mechanism.

## CONCLUSIONS

Collision-induced dissociation (CID) mass spectrometry experiments in conjunction with density functional theory (DFT) and MP2 calculations were used to gain insight into the molecular structure and dissociation channels of uranyl species containing acetone and diacetone alcohol ligands. Uranyl complexes with isotopically labeled ligands were prepared by electrospray ionization and gas-phase exchange reactions. Comparison of the CID spectra with previous results[4] clearly shows that the previously observed "$[UO_2(ACO)_{6,7,8}]^{2+}$" species contained DAA ligands. MP2 and DFT calculations confirm that species can form stable complexes with DAA bonded in either bidentate or monodentate fashion but that the effective number of atoms coordinating with uranium in the equatorial plane does not exceed five. The "$[UO_2(ACO)_7]^{2+}$" and "$[UO_2(ACO)_8]^{2+}$" species are shown to be the stable $[UO_2(ACO)_1(DAA)_3]^{2+}$ and $[UO_2(DAA)_4]^{2+}$ species. For the latter species, three DAA ligands bind in a monodentate and one DAA binds in a bidentate fashion. The presence of DAA ligands coordinating with uranyl in the complexes also provides an explanation for the observed water-elimination reactions. Experimental data show that dipositive uranyl species with DAA ligands can form mesityl oxide through elimination of water and monopositive alkoxide species through elimination of a proton. MP2 calculations suggest that $[UO_2(DAA)_2]^{2+}$ could form alkoxide species and $[UO_2(DAA)_3]^{2+}$ could form MOX, but these reactions are not observed by experiment. Experiment and MP2 calculations agree that $[UO_2(ACO)_1(DAA)_2]^{2+}$ produces both MOX and alkoxide, suggesting that the crowding of ligands around uranyl affects the reaction channels.

## ASSOCIATED CONTENT

### Supporting Information

Cartesian coordinates, absolute energies, and zero-point energies for optimized structures. This material is available free of charge via the Internet at http://pubs.acs.org.

## AUTHOR INFORMATION


### Corresponding Author

*E-mail: bert.dejong@pnnl.gov, JKGibson@lbl.gov, twindus@iastate.edu.

### Author Contributions

The manuscript was written through contributions of all authors. All authors have given approval to the final version of the manuscript.

### Author Contributions

‡This author was the primary contributor for the experiment.

### Author Contributions

‖This author was the primary contributor for the computational modeling.


### Notes

The authors declare no competing financial interest.

## ACKNOWLEDGMENTS

Research sponsored by the U.S. Department of Energy, Office of Basic Energy Sciences, Heavy Element Chemistry Program at LBNL under Contract No. DE-AC02-05CH11231 [D.R., J.K.G.] and at PNNL under Contract No. DE-AC05-76RL01830 [W.A.d.J.]. Funding has been provided by Iowa State University and an NSF grant for petascale applications. Part of this research was performed at the Ames Laboratory, FWP AL-08-330-039. Ames Laboratory is managed by Iowa State University for the U.S. Department of Energy under contract DE-AC02-07CH11358. Part of this research was performed in part using the Molecular Science Computing capability at the EMSL, a National scientific user facility sponsored by the U.S. Department of Energy's Office of Biological and Environmental Research and located at the PNNL, operated for the Department of Energy by Battelle.

## REFERENCES


(1) de Jong, W. A.; Apra, E.; Windus, T.; Nichols, J. A.; Harrison, R. J.; Gutowski, K. E.; Dixon, D. A. *J. Phys. Chem. A* **2005**, *109*, 11568.
(2) Groenewold, G. S.; Oomens, J.; de Jong, W. A.; Gresham, G. L.; McIlwain, M. E.; Van Stipdonk, M. J. *Phys. Chem. Chem. Phys.* **2008**, *10*, 1192.
(3) Groenewold, G.; de Jong, W. A.; Oomens, J.; Van Stipdonk, M. *J. Am. Soc. Mass Spectrom.* **2010**, *21*, 719.
(4) Rios, D.; Rutkowski, P. X.; Van Stipdonk, M. J.; Gibson, J. K. *Inorg. Chem.* **2011**, *50*, 4781.
(5) Schoendorff, G.; de Jong, W. A.; Van Stipdonk, M. J.; Gibson, J. K.; Rios, D.; Gordon, M. S.; Windus, T. L. *Inorg. Chem.* **2011**, *50*, 8490.
(6) Rutkowski, P. X.; Michelini, M. C.; Bray, T. H.; Russo, N.; Marcalo, J.; Gibson, J. K. *Theor. Chem. Acc.* **2011**, *129*, 575.
(7) Shvartsburg, A. A.; Wilkes, J. G. *Int. J. Mass Spectrom.* **2003**, *225*, 155.
(8) Rutkowski, P. X.; Rios, D.; Gibson, J. K.; Van Stipdonk, M. J. *J. Am. Soc. Mass Spectrom.* **2011**, *22*, 2042.
(9) Gronert, S. *J. Am. Soc. Mass Spectrom.* **1998**, *9*, 845.
(10) Valiev, M.; Bylaska, E.; Govind, N.; Kowalski, K.; Straatsma, T.; Van Dam, H.; Wang, D.; Nieplocha, J.; Apra, E.; Windus, T.; de Jong, W. *Comput. Phys. Commun.* **2010**, *181*, 1477.
(11) Bergner, A.; Dolg, M.; Kuchle, W.; Stoll, H.; Preuss, H. *Mol. Phys.* **1993**, *80*, 1431.
(12) Kuchle, W.; Dolg, M.; Stoll, H.; Preuss, H. *Mol. Phys.* **1991**, *74*, 1245.
(13) Kuchle, W.; Dolg, M.; Stoll, H.; Preuss, H. *J. Chem. Phys.* **1994**, *100*, 7535.
(14) Godbout, N.; Salahub, D. R.; Andzelm, J.; Wimmer, E. *Can. J. Chem.* **1992**, *70*, 560.
(15) Slater, J. C. *Phys. Rev.* **1951**, *81*, 385.
(16) Vosko, S. H.; Wilk, L.; Nusair, M. *Can. J. Phys.* **1980**, *58*, 1200.
(17) Becke, A. D. *J. Chem. Phys.* **1993**, *81*, 5.
(18) Lee, C.; Yang, W.; Parr, R. G. *Phys. Rev. B* **1988**, *37*, 785.
(19) Grimme, S. *J. Chem. Phys.* **2006**, *124*, 16.
(20) Coetzee, J. F.; Chang, T. H. *Pure Appl. Chem.* **1986**, *58*, 1541.
(21) Wahl, J. H.; Bolz, C. D.; Wahl, K. L. *Lc Gc N. Am.* **2010**, *28*, 1042.
(22) Kim, Y. K.; Hatfield, J. D. *J. Chem. Eng. Data* **1985**, *30*, 149.
(23) Schoendorff, G.; Windus, T.; de Jong, W. A. *J. Phys. Chem. A* **2009**, *113*, 12525.